Unexpected phenotypic and molecular changes of combined glucocerebrosidase and acid sphingomyelinase deficiency

Marcus Keatinge[1,2,3,*], Matthew E. Gegg[4], Lisa Watson[1,2], Heather Mortiboys[2], Nan Li[1,2], Mark Dunning[2], Deepak Ailani[1,2], Hai Bui[5], Astrid van Rens[6], Dirk J. Lefeber[6,7], Anthony H.V. Schapira[4], Ryan B. MacDonald[1,*,‡,§], Oliver Bandmann[1,2,*,‡]

[1]Bateson Centre, Firth Court, University of Sheffield, Western Bank Sheffield S10 2TN, UK
[2]Sheffield Institute for Translational Neuroscience (SITraN), University of Sheffield, 385a Glossop Road, Sheffield S10 2HQ, UK
[3]Centre for Discovery Brain Sciences, Chancellor's Building, Edinburgh EH16 4TJ, UK
[4]Department of Clinical and Movement Neurosciences, UCL Queen Square Institute of Neurology, London NW3 2PF, UK
[5]Eli Lilly and Company, Drop Code 1940,Indianapolis, IN 46285 USA
[6]Department of Laboratory Medicine, Translational Metabolic Laboratory, Radboud University Medical Center, Nijmegen, The Netherlands
[7]Department of Neurology, Donders Institute for Brain, Cognition and Behaviour, Radboud University Medical Centre, Nijmegen, The Netherlands

[*]Authors for correspondence: Mkeatinge2@exseed.ed.ac.uk; ryan.macdonald@ucl.ac.uk; o.bandmann@sheffield.ac.uk.
[‡]Joint senior authors of this work.
[§]Present address: Institute of Ophthalmology, University College London, 11-43 Bath St, Greater London EC1V 9EL.

Summary Statement

Simultaneous inhibition of *gba1* and *smpd1* gene function (both implicated in Parkinson's Disease) unexpectedly rescues neuronal gene expression, mitochondrial defects and extends the lifespan of *gba1* mutant zebrafish.

Abstract

Heterozygous variants in *GBA1* encoding glucocerebrosidase (GCase) are the most common genetic risk factor for Parkinson's disease (PD). Moreover, sporadic PD patients also have a substantial reduction of GCase activity. Genetic variants in *SMPD1* are also overrepresented in PD cohorts, whilst a reduction of its encoded

Disease Models & Mechanisms • DMM • Accepted manuscript

enzyme (ASM) activity is linked to an earlier age of PD onset. Despite both converging on the ceramide pathway, how combined deficiencies of both enzymes may interact to modulate PD has yet to be explored. Therefore, we created a double knock out (DKO) zebrafish line for both *gba1* and *smpd1* to test for an interaction *in vivo,* hypothesising an exacerbation of phenotypes in the DKO compared to single mutants. Unexpectedly, DKOs maintained conventional swimming behaviour and had normalised neuronal gene expression signatures when compared to single mutants. We further identified rescue of mitochondrial Complexes I and IV in DKOs. Despite having an unexpected rescue effect, our results confirm ASM as a modifier of GBA1 deficiency *in vivo.* Our study highlights the need for validating how genetic variants and enzymatic deficiencies may interact *in vivo*.

Keywords: Parkinson's disease, glucocerebrosidase 1, acid sphingomyelinase, zebrafish, gene-gene interaction.

INTRODUCTION

There is compelling evidence of an excessive burden of lysosomal disease gene variants and lysosomal dysfunction in PD.[1,2] Bi-allelic mutations in *glucocerebrosidase 1* (*GBA1)* cause the lysosomal storage disorder (LSD) Gaucher's disease (GD), whilst heterozygous mutations are the most common and strongest genetic risk factor for sporadic PD, with a prevalence of ~ 5-20% depending on the population investigated.[3–5] PD patients also exhibit reduced GCase activity in different tissues, including the brain[6], regardless of their *GBA1* mutation status.[6–8]

In a similar fashion to *GBA1* mutations, homozygous *SMPD1* mutations (encoding acid sphingomyelinase, ASM) also cause an LSD, in this case Niemann Pick disease while heterozygous *SMPD1* variants are associated with increased risk of sporadic PD.[9–13] Due to their rarity within the PD population, the functional significance of these *SMPD1* variants is still not completely understood.[9,14] However, a reduction of ASM activity is correlated with an earlier age of disease onset in PD, as well as in other synucleinopathies including dementia with Lewy bodies and multiple system atrophy.[9,14] Both *GBA1* and *SMPD1* encode lysosomal enzymes that converge on ceramide metabolism (Figure 1). Therefore, an additive interaction between these two enzymes is biologically plausible and but awaits experimental confirmation. We hypothesised that ASM deficiency could worsen the functional consequences of GCase deficiency, aggravating phenotypes which could potentially lead to, or enhance, neurodegeneration.

Zebrafish (*Danio rerio*) are an attractive vertebrate model to study the biological effect of both monogenic PD genes and genetic risk factors for PD[15–17], including *gba1* deficiency.[18] We had previously characterised a *gba1* mutant zebrafish line *(gba1*$^{-/-}$*),*[19] and demonstrated its usefulness to study gene-gene interactions.[20] *gba1*$^{-/-}$ zebrafish faithfully model key features of GCase deficiency/Gaucher's disease, including Gaucher cell accumulation, marked inflammation with microglial infiltration, mitochondrial dysfunction and neurodegeneration.[19] *gba1*$^{-/-}$ larvae develop normally but *gba1*$^{-/-}$ juvenile zebrafish then rapidly deteriorate from 10-12 weeks onwards and die between 12 and 14 weeks.

As expected, combined GCase and ASM deficiency acted synergistically on key sphingolipid metabolites in the *gba1*$^{-/-}$;*smpd1*$^{-/-}$ double-mutant zebrafish. However, instead of a worsening of phenotypes, we unexpectedly observed markedly prolonged survival and conventional swimming behaviour in *gba1*$^{-/-}$;*smpd1*$^{-/-}$ mutants compared to the *gba1*$^{-/-}$ (single) mutant zebrafish. RNAseq-based pathway analysis confirmed restoration of neuronal health in *gba1*$^{-/-}$*;smpd1*$^{-/-}$ compared to the *gba1*$^{-/-}$. Mechanistic experiments identified a rescue effect of combined GCase and ASM deficiency on mitochondrial Complexes I and IV function in *gba1*$^{-/-}$;*smpd1*$^{-/-}$ compared to the marked but distinct mitochondrial dysfunction in *gba1*$^{-/-}$ or *smpd1*$^{-/-}$ single mutant zebrafish. The mitochondrial rescue led to an abrogation of oxidative membrane damage, further reflecting the overall restorative effect of ASM deficiency on neuronal health in GCase deficiency. Our study highlights the need of functional, mechanistic validation for the interaction of any putative genetic/enzymatic risk factors for human diseases in suitable model systems, rather than readily assuming an additive effect.

Methods

Zebrafish husbandry

All larval and adult zebrafish were housed at the University of Sheffield; experimental procedures being in accordance UK Home Office Animals (Scientific Procedures) Act 1986 (Project license PPL 70/8437, held by Dr Oliver Bandmann). Adult zebrafish were housed at a density of 20 per tank, on a cycle of 14 h of light, 10 h of dark. Adults and embryos were kept at constant temperature of 28°C.

Mutant line generation and line maintenance

The gba1$^{-/-}$ mutant lines was generated using TALEN technology.[19] The *smpd1*$^{-/-}$ mutant line was generated by the Crispr/Cas9 method as previously described.[21,22] The following ultramer template was used: 5'-

AAAGCACCGACTCGGTGCCACTTTTTCAAGTTGATAACGGACTAGCCTTATTTTA ACTTGCTATTTCTAGCTCTAAAACGGATTGAGGCTTGTGTCTCCCTATAGTGAGT CGTATTACGC. The *smpd1*$^{-/-}$ line was genotyped using primers F 5'-AGCCGTGGTGGTTTCTACAG and R 5'-CCTTCTCTCCCTTGTTCTCG. The *smpd1*$^{-/-}$ line was crossed to *gba1*$^{+/-}$ to generate double heterozygous individuals. These were subsequently in-crossed to generate double mutants, single mutants and WT controls. At each in-cross larvae were genotyped at 3 days post-fertilisation (dpf) by larval tail biopsy as previously described.[23] Each genotype was raised in genotype-specific tanks at a density of 10-15 fish per tank. All individuals were re-genotyped at 10 weeks post-fertilisation. For survival curves, animals were culled for humane reasons when they could no longer maintain consistent buoyancy.

Immunohistochemistry

WT and mutant fish were fixed in 4% paraformaldehyde overnight at 4°C before removal of the eye, which was incubated in 30% sucrose in PBS overnight at 4°C. Eyes were then embedded in OCT and cryosectioned at 20um (Leica). Slides were rehydrated in PBS before blocked for 1 hour at room temperature using 150 µl block (1% sheep serum, 5% BSA, 0.3% Triton-X, 0.1% Tween-20 in PBS). Slides were then incubated with 150 µl primary antibody solution (4.C.4; 1:50 dilution in block solution; Antibody registry ID: AB_10013752) overnight at 4°C. After incubation slides were washed 3 times in PBS for 20 minutes followed by incubation with secondary antibody (Alexa anti-mouse-647; A-21235) for 2 hours. Slides were then washed in PBS 3x20min, before adding Fluoroshield with DAPI (Sigma; F6057-20ML) and applying a glass coverslip. Slides were imaged on a Zeiss LSM 900 confocal microscope using a 40x water immersion objective.

Biochemical activity assays and mass spectrometry

ASM activity was determined using homogenates prepared as follows. Tubes containing twenty embryos (5 dpf) were sonicated in 500 µl MilliQ and centrifuged (11000 rpm). 20 µL of supernatant was incubated with substrate HMU-PC (6-hexadecanoylamino-4-methylumbelliferyl-phosphorylcholine 0.66 mM, 20 µL, Moscerdam Substrates, NL) at pH 5.2 and 37 °C for 2 hours. Fluorescence intensity was measured at 415 (ex) and 460 (em) nm using a plate reader (LS55, Perkin Elmer). Lysosomal and mitochondrial enzyme assays as well as mass spectrometry were undertaken as previously described.[19]

Lipid peroxidation assay

We were unable to isolate enough mitochondria from brain tissue to robustly measure lipid peroxidation signals above background levels. However, enough mitochondria could be isolated from 3-month-old adult zebrafish bodies to perform the assay robustly. Bodies were homogenised in ice cold mitochondrial isolation buffer. The Abcam lipid peroxidation kit (ab118970) fluorometric assay was used to measure lipid peroxidation according to manufacturer's instructions. Results were normalised to WT.

RNA preparation for gene expression analysis

RNA was prepared from brain tissue of 12 weeks old zebrafish. A Trizol based protocol was used to extract RNA from the tissue. Briefly, individual brains were homogenized in 250 µl TRI Reagent (Sigma) and incubated at room temperature before adding 50 µl chloroform (Thermo Fisher). The samples were centrifuged at 13,300 x g and the top aqueous phase was collected and transferred to a separate tube. RNA was precipitated from the aqueous phase by mixing with equal volume of isopropanol (Thermo Fisher) and centrifugation at 13,300 x g. Precipitated RNA was resuspended in DEPC-treated water (Thermo Fisher) and its concentration and quality were quantified using the Nanodrop 1000 Spectrophotometer. 750 ng of high quality total RNA, with an RNA integrity number (RIN) of 9 or above, was used in the preparation of sequencing libraries using the NEB Ultra II Directional RNA Library Prep Kit (NEB catalogue number E7760), following the polyA mRNA workflow. Libraries were individually indexed and pooled for sequencing. Single-end 100bp sequencing was performed on the Illumina HiSeq 2500 platform using Rapid Run mode with V2 chemistry.

RNA-seq Analysis

Raw sequencing reads were processed using the bcbio workflow system. The quality of the samples was checked using FastQC and multiqc. The salmon tool (v0.9.01) was used to quantify genes from the zebrafish reference transcriptome (Danio_rerio.GRCz11.98.gtf from Ensembl.org).[24] The salmon files were then imported into R using the tximport Bioconductor package.[25] Unsupervised clustering and PCA with DESeq2 revealed a batch effect corresponding to sample preparation date.[26] Differential expression was performed using DESeq2 incorporating a batch factor into the model. The contrast tested was between *gba1*$^{-/-}$, double mutants and WT; a positive log fold-change indicating higher expression in GBA single mutants. The clusterProfiler Bioconductor package was used to identify enriched pathways in

up- (adjusted p-value less than 0.05 and log fold-change > 1) and down-regulated genes (adjusted p-value less than 0.05 and log2 fold-change <-1).[27]

Gene set enrichment analysis

The analysis was performed with Gene Set Enrichment Analysis (GSEA) software version 4.0.3 (https://www.gsea-msigdb.org/gsea/index.jsp). GSEA preranked analysis was used with default settings except for "Collapse/Remap to gene symbols" set to "No_Collapse". A ranked list used for the analysis was calculated with each gene assigned a score based on the adjusted p value and the log2 fold change. Zebrafish lysosomal and mitochondrial gene sets were prepared by identifying zebrafish homologues of the genes in human genes sets in Molecular Signatures Database (MSigDB) v7.1.

Statistical analysis

Graphpad prism V.6 software (Graphpad) was used for statistical analysis and all error bars shown denote the mean ± SD of the mean. All experiments were performed in biological triplicate unless otherwise stated. All data were analysed with either T test, two-way ANOVA. Significance in all enzyme activity assays was determined by two way ANOVA with Tukey's multiple comparison test.

Results

***smpd1*$^{-/-}$ zebrafish display abolished acid sphingomyelinase activity and marked sphingolipid accumulation**

We initially hypothesised that deficiency of both GCase and ASM enzymes may synergise, leading to a further aggravation of *gba1* deficient phenotypes *in vivo*. To address this, we identified a single *smpd1* orthologue in zebrafish (ENSDARG00000076121) with 59% shared identity to the human *SMPD1* gene at both the DNA and the protein level. CRISPR/Cas9 technology was used to generate a *smpd1* stable mutant line *(smpd1*$^{-/-}$*).* The selected mutant allele contained a 5bp deletion and 136bp insertion within exon 3, resulting in a frame-shift and the generation of a premature stop codon (Figure 2A and Supplemental Figure S1). Enzymatic activity of ASM in *smpd1*$^{-/-}$ at 5 dpf was reduced by 93% (p=0.006, Figure 2B). The large reduction in ASM enzymatic activity resulted in a significant increase of key glycolipid substrates in the *smpd1*$^{-/-}$ larvae already at 5 dpf (Figure 2C). The *smpd1*$^{+/-}$ line was crossed with *gba1*$^{+/-}$ to generate *gba1*$^{+/-}$*; smpd1*$^{+/-}$. The latter were subsequently in-crossed to generate double mutants, single mutants and WT controls for all subsequent experiments. At each in-cross larvae were genotyped at 3

days post-fertilisation (dpf) and then raised in genotype-specific tanks. Every genotype was present in its expected mendelian ratio (1/16th) during genotyping at larval stages (Supplemental table 1), but only WT, *gba1*$^{-/-}$, *smpd1*$^{-/-}$ and *gba1*$^{-/-}$;*smpd1*$^{-/-}$ were raised for experiments.

Combined ASM and GCase deficiency synergistically increases sphingolipid metabolites

We had previously reported marked sphingolipid accumulation in *gba1*$^{-/-}$ zebrafish.[19] We hypothesised that combined (enzymatic) GCase and ASM deficiency would synergistically increase distinct sphingolipid subtypes. Using mass spectrometry, a comprehensive panel of glycolipid substrates was analysed in the brains of *gba1*$^{-/-}$ and *smpd1*$^{-/-}$ single mutant as well as in *gba1*$^{-/-}$;*smpd1*$^{-/-}$ double mutant zebrafish and WT controls at 12 weeks of age. As expected, a marked additive effect of combined GCase and ASM deficiency was observed for Glucosylceramide levels (the direct substrate of GCase) (Figure 3A). This was likely due to both a block in Glucosylceramide catabolism and also due to metabolic compensation in the flux of sphingolipid generation. Combined GCase and ASM deficiency also resulted in an additive effect on lactosylceramide, ceramide and sphinganine levels (Figure 3B-D). Sphingosine levels were increased in *gba1*$^{-/-}$;*smpd1*$^{-/-}$ compared to WT, reflecting an increase compared to *gba1*$^{-/-}$ but not compared to *smpd1*$^{-/-}$ (Figure 3E). Unexpectedly, there was no synergistic effect in sphingomyelin levels in the *gba1*$^{-/-}$;*smpd1*$^{-/-}$ double mutants (Figure 3F).

The inflammation markers chitotriosidase and β-Hexosaminidase are markedly increased in the serum of GD patients and used as biomarkers to monitor disease activity.[28] We previously observed a marked increase in chitotriosidase and β-hexosaminidase activity in *gba1*$^{-/-}$ zebrafish brain tissue at 12 weeks.[19] As key GCase substrates were synergistically increased in *gba1*$^{-/-}$;*smpd1*$^{-/-}$ double mutant zebrafish, we investigated whether combined GCase and ASM inactivation may also result in a further increase of chitotriosidase and β-hexosaminidase activity. Unexpectedly, *gba1*$^{-/-}$;*smpd1*$^{-/-}$ double mutant zebrafish displayed a similar increase in chitotriosidase and β-hexosaminidase activity compared to *gba1*$^{-/-}$ (Supplemental Figure 2). Furthermore, we had previously detected Gaucher cell invasion in the CNS of end stage *gba1*$^{-/-}$.[18] Analyses of the retinas across all genotypes demonstrated similar Gaucher cell invasion in the double mutants (Figure 4) with both *gba1*$^{-/-}$ and *gba1*$^{-/-}$;*smpd1*$^{-/-}$ double mutants showing a ~50% increase in 4C4 positive cells compared to WT. These 4C4 cells in both *gba1*$^{-/-}$ and *gba1*$^{-/-}$;*smpd1*$^{-/-}$ double mutants

also tended to be larger and rounder, indicative of the Gaucher cells we had previously described. These data suggest persistent yet unaltered neuroinflammatory states in the double mutants despite a marked synergistic increase in sphingolipid metabolites.

ASM deficiency unexpectedly prolongs survival in GCase deficiency

The marked additive effect of combined GCase and ASM deficiency on sphingolipid levels led us to hypothesize that ASM deficiency would further worsen the motor phenotype and shorten survival in *gba1*$^{-/-}$;*smpd1*$^{-/-}$ double mutant zebrafish. Unexpectedly, genetic inactivation of ASM led to a complete rescue of this behaviour in the *gba1*$^{-/-}$;*smpd1*$^{-/-}$ double mutant zebrafish (Supplemental Movies S1 (WT), S2 (*smpd1*$^{-/-}$), S3 (*gba1*$^{-/-}$) and S4 (*gba1*$^{-/-}$;*smpd1*$^{-/-}$)). Importantly, disease free survival, where animals could consistently maintain buoyancy, was also markedly increased by 22% in *gba1*$^{-/-}$;*smpd1*$^{-/-}$ double mutant zebrafish compared to *gba1*$^{-/-}$ (median survival of 102 dpf in *gba1*$^{-/-}$ and 125dpf in *gba1*$^{-/-}$;*smpd1*$^{-/-}$, p=0.0055, Figure 5A). Despite not exhibiting the same barrel rolling phenotype as the *gba1*$^{-/-}$, and could also maintain their buoyancy, the *gba1*$^{-/-}$;*smpd1*$^{-/-}$ double mutants would ultimately be found unresponsive at the bottom of the tank and so were culled for humane reasons. We also raised *smpd1*$^{-/-}$ to determine its lifespan, but never encountered a decrease in viability compared to WT, even up to the age of 18 months (data not shown).

***RNAseq base pathway analysis confirms restored neuronal health in gba1*$^{-/-}$*;smpd1*$^{-/-}$**

We next applied RNAseq-based pathway analysis to further elucidate the underlying mechanisms of the observed rescue effect. The differential gene expression analysis all four genotypes (wild type, *gba1*$^{-/-}$ and *smpd1*$^{-/-}$ single mutants, *gba1*$^{-/-}$;*smpd1*$^{-/-}$ double mutants) identified a total of 512 genes which were dysregulated in *gba1*$^{-/-}$ but rescued in *gba1*$^{-/-}$;*smpd1*$^{-/-}$. Amongst these, there are a downregulation of 219 genes and an upregulation of 293 genes in *gba1*$^{-/-}$ compared to wild-type and *gba1*$^{-/-}$;*smpd1*$^{-/-}$ (adjusted p-value ≤0.05, |log2Fold change| ≥1). We next employed ClusterProfiler analysis on gene ontology (GO) categories to identify functionally relevant pathways within the rescued gene sets. Key neuronal pathways including the GO terms for synaptic signalling, chemical synaptic transmission and calcium ion regulated exocytosis were markedly downregulated in *gba1*$^{-/-}$ but normalised in *gba1*$^{-/-}$;*smpd1*$^{-/-}$ (Figure 5B). This suggests that key aspects of neuronal function were restored in the *gba1*$^{-/-}$;*smpd1*$^{-/-}$ double mutants.

We also observed an enrichment of upregulated genes in *gba1*$^{-/-}$compared to *gba1*$^{-/-}$*;smpd1*$^{-/-}$ in a broad range of GO terms, the top 5 of which thought to regulate muscle function. However, since our RNA-seq analysis was carried out on brain tissue, we consider these changes to be of limited relevance only (Supplementary Figure 3). Upregulation of the inflammatory signature in *gba1*$^{-/-}$ was retained in the *gba1*$^{-/-}$*;smpd1*$^{-/-}$ but not further enhanced (data not shown).

As both GCase and ASM are lysosomal hydrolases, we specifically focused on the effect of isolated GCase deficiency in *gba1*$^{-/-}$ compared to combined GCase and ASM deficiency in *gba1*$^{-/-}$*;smpd1*$^{-/-}$ on lysosome transcriptomic pathways. Gene set enrichment analysis led to the identification of 27 leading-edge, dysregulated lysosomal genes, which account for the pathway's enrichment signal. The expression of these 27 lysosomal genes was increased in *gba1*$^{-/-}$ compared to wild-type and *gba1*$^{-/-}$*;smpd1*$^{-/-}$ (Figure 5C, Supplementary Table 2). Amongst these 27 genes, acid hydrolases contributed the most. Cathepsin L, involved in the initiation of protein degradation, ranked as the top rescued gene. The apparent normalisation of lysosomal gene expression profiles in *gba1*$^{-/-}$*;smpd1*$^{-/-}$ was in contrast to the observed marked increase in a wide range of sphingolipid levels in *gba1*$^{-/-}$*;smpd1*$^{-/-}$ compared to *gba1*$^{-/-}$ *or smpd1*$^{-/-}$ single mutants (see above).

We had previously observed marked mitochondrial dysfunction in *gba1*$^{-/-}$. We therefore also focussed on the analysis of mitochondrial genes involved in the oxidative phosphorylation pathway. This leading-edge mitochondrial gene subset included 16 genes encoding the subunits of the Complex I, II, IV and V in mitochondrial electron transport chain (Supplementary Table 3). Interestingly, gene set enrichment analysis showed an upregulation of this mitochondrial gene subset in *gba1*$^{-/-}$, presumably as a compensatory mechanism to the impaired function of the mitochondrial respiratory chain, but similar mitochondrial gene expression levels in wild-type and *gba1*$^{-/-}$*;smpd1*$^{-/-}$(Figure 5D).

***Restoration of mitochondrial Complex I and IV function in gba1*$^{-/-}$*;smpd1*$^{-/-}$**

We next compared the mitochondrial respiratory chain function across all four genotypes to further determine whether the normalised gene expression levels for oxidative phosphorylation-related genes would be reflected in normalised mitochondrial function. Complex I activity was reduced by 65% in *smpd1*$^{-/-}$ compared to WT levels (p=0.0198, Figure 5A) but restored to 92% of WT levels in *gba1*$^{-/-}$*;smpd1*$^{-/-}$ (p=0.0445, Figure 6A). Complex II was not significantly altered in any of the

genotypes (Figure. 6B). Complex III activity in *gba1*$^{-/-}$ was reduced by 45% compared to WT levels (p=0.0091, Figure 6C) as previously observed.[19] Complex III activity in the *gba1*$^{-/-}$;*smpd1*$^{-/-}$ double mutant zebrafish was reduced by only 9% compared to WT levels however this did not reach significance when compared to *gba1*$^{-/-}$ (p=0.1688). Complex IV activity was unchanged in *smpd1*$^{-/-}$ compared to WT, but reduced by 40% in *gba1*$^{-/-}$ compared to WT as previously reported (p=0.0491, Figure 6D). Remarkably, there was a marked improvement of complex IV activity in *gba1*$^{-/-}$;*smpd1*$^{-/-}$ with an increase in activity of 69% compared to *gba1*$^{-/-}$ (p= 0.0005, Figure 6D). Thus, there is rescue of mitochondrial respiratory chain function in mitochondrial Complex I and IV, where ASM deficiency normalises mitochondrial Complex IV function in *gba1*$^{-/-}$ and GCase deficiency normalises mitochondrial Complex I function in *smpd1*$^{-/-}$. Malfunction of the mitochondrial respiratory chain can result in oxidative stress and subsequent lipid peroxidation. We therefore investigated next whether the observed rescue in mitochondrial Complex I and IV results in reduced oxidative stress-related damage. Mitochondrial lipid peroxidation was increased in whole *gba1*$^{-/-}$ adult fish by 63% above WT levels (p= 0.0214, Figure 6E). As predicted, lipid peroxidation levels were reduced by 70% in *gba1*$^{-/-}$;*smpd1*$^{-/-}$ double mutants compared to *gba1*$^{-/-}$ and thus effectively normalised (p=0.0094, Figure 6E).

Discussion

Biochemically, GCase and acid sphingomyelinase both play a key role in sphingolipid metabolism.[29,30] Unexpectedly, we observed a rescue of motor behaviour and a marked prolongation of life expectancy following combined GCase and ASM deficiency, despite clear evidence of an additive effect on the intracellular level of key sphingolipids and their metabolites. The remarkable rescue effect of mitochondrial Complex I and IV in *gba1*$^{-/-}$;*smpd1*$^{-/-}$ on behaviour and survival suggests a central role of mitochondrial dysfunction in GCase deficiency. The profound normalisation of neuronal function in *gba1*$^{-/-}$;*smpd1*$^{-/-}$, as indicated in our RNA-seq based pathway analysis, is in keeping with the observation of the rescued motor phenotype. The normalisation of intracellular homeostasis is also reflected by the normalisation of both lysosomal and mitochondrial transcriptional pathways.

Mitochondrial dysfunction is a key feature of both familial and sporadic PD as well as in LSD's, the mitochondrial network and lysosomal system are also known to be tightly interlinked.[31–36] ASM activity must also be tightly controlled, as either too much or too little has been shown to negatively affect mitochondrial function, depending on the cell type, tissue or experimental paradigm understudy[37–39]. However, when

focussed on neuronal health, ASM inhibition consistently ameliorates phenotypes in the context of neuronal loss.[39–41] A plausible rescue mechanism of mitochondrial function in DKO, could be glutamate/calcium signalling. Neuronal GCase deficiency *in vitro* has been shown to sensitise mitochondria to physiological levels of glutamate.[33] This leads to pathological responses in calcium signalling and downstream mitochondrial dysfunction[33]. Conversely, ASM deficiency *in vitro* has been shown to cause a decreased vulnerability to glutamate linked excitotoxicity in neurons.[42] This was not only linked to a decrease in intracellular calcium levels, but also of oxidative stress.[42] Inhibiting ASM function in primary oligodendrocyte culture, can also rescue glutamate induced mitochondrial dysfunction.[39]

Of note, 9 genes involved in calcium ion regulated exocytosis were downregulated in *gba1*$^{-/-}$ single mutants but subsequently normalised in the DKO, namely syt*2a*, *syt7a*, *cplx3a*, *cadpsa*, *snap47 cacna1hb, rims1b, cbarpb, napbb*.

An alternative mechanism could be intracellular redistribution of the sphingolipid profile in double mutants. We only detected a synergistic increase in sphingolipid levels in DKO compared to single *gba1*$^{-/-}$, but not a normalisation. However, this does not exclude an effect on subcellular localisation of a specific sphingolipid metabolite which may underpin the observed rescue mechanism. Sphingolipid signalling is vitally important for many varied inter- and intracellular processes.[29] Sphingolipid signalling must remain highly compartmentalised due to its pleiotropic effects.[43–45] However, due to technical reasons we used bulk brain tissue for our metabolite analysis, which would therefore not allow for the detection inter- and intracellular sphingolipid differences. Future work should involve metabolic analyses of sphingolipids separated by cell type and by specific cellular fractions, to produce a spatial understanding of the distinct sphingolipid metabolism and distribution across the different *gba1*$^{-/-}$/*smpd1*$^{-/-}$ genotypes. Furthermore, whole body analyses using recently developed techniques to monitor in-situ glucosylceramide generation would give novel insights into the glycolipid dysregulation in our double mutants.[46]

Intriguingly, deficiency of another LSD gene, *asah1,* which functions on a separate arm of the ceramide pathway to *smpd1* (Figure 1), also ameliorates *gba1* deficient phenotypes *in vivo* and *in vitro*. Biallelic *ASAH1* mutations cause the LSD Farber disease in humans. By developing a DKO zebrafish for *gba1*$^{-/-}$ and *asah1*$^{-/-}$, Lelieveld and colleagues demonstrated that *asah1* deficiency also led to a rescue of behavioural and neuronal phenotypes in a similar manner to our DKO *gba1*$^{-/-}$;*smpd1*$^{-/-}$

zebrafish.[47] In keeping with our own data, the rescue effect observed was not due to an amelioration of neuroinflammation, as DKO retained the upregulation of *tnfβ, il1β* and *apoeb* exhibited by *gba1*$^{-/-}$.[47] Similarly, Kim *et al* demonstrated that pharmacological inhibition of ASAH1 led to a significant reduction in *GBA1* linked cellular phenotypes including accumulation of ubiquitinated proteins and alpha synuclein in dopaminergic neuronal cultures derived from PD-GBA1$^{+/-}$ patients.[48]

For practical reasons, we modelled combined enzymatic deficiency using homozygous, and not heterozygous mutants for *gba1* and *smpd1*, intrinsically modelling LSDs and not PD. However, the unexpected nature of our results demonstrates the need for future characterisation of combined partial LSD gene deficiencies in the wider context of PD.

Abbreviations

Parkinson's Disease (PD), Glucocerebrosidase 1 (GBA1), acid sphingomyelinase (SMPD1), Glucocerebrosidase enzyme (GCase), Acid Sphingomyelinase enzyme (ASM), Genome Wide Association Study (GWAS), Lysosomal storage disorder (LSD), RNA Integrity Number (RIN), Gene Set Enrichment (GSEA), Double Knockout (DKO).

Supplemental data

Supplemental data can be found online at

Declaration

Ethics approval and consent to participate

All larval and adult zebrafish were housed at the University of Sheffield; experimental procedures being in accordance UK Home Office Animals (Scientific Procedures) Act 1986 (Project license PPL 70/8437, held by Dr Oliver Bandmann).

Consent for publication

Not applicable.

Availability of data and materials

All data generated or analysed during this study are included in this published article [and its supplementary information files]. The exception is the raw data of the gene expression which is available from the corresponding author on reasonable request.

Competing interests

The authors declare that they have no competing interests

Funding

This work was supported by funding from Parkinson's UK (G1404 and G1704), the Medical Research Council (MRC, MR/R011354/1 and MR/M006646/1). RBM is supported by a BBSRC David Phillips Fellowship (BB/S010386/1). This research was also supported by the NIHR Sheffield Biomedical Research Centre (BRC).

Authors' contributions

Conducted and analysed experiments: MK, MG, LW, HM, NL, MD, DA, HB, AR
Experimental design: MK, MG, LW, HM, NL, MD, DA, HB, AR, DL, RM, AS, OB
MK and OB wrote the manuscript.
All authors read and approved the final manuscript

Acknowledgements

This work was supported by funding from Parkinson's UK (G1404 and G1704), the Medical Research Council (MRC, MR/R011354/1 and MR/M006646/1). RBM was supported by a BBSRC David Phillips Fellowship (BB/S010386/1). This research was also supported by the NIHR Sheffield Biomedical Research Centre (BRC).

References:

1. Robak, L. A. *et al.* Excessive burden of lysosomal storage disorder gene variants in Parkinson's disease. *Brain* (2017). doi:10.1093/brain/awx285
2. Wallings, R. L., Humble, S. W., Ward, M. E. & Wade-Martins, R. Lysosomal Dysfunction at the Centre of Parkinson's Disease and Frontotemporal Dementia/Amyotrophic Lateral Sclerosis. *Trends Neurosci.* **42**, 899–912 (2019).
3. Siebert, M., Sidransky, E. & Westbroek, W. Glucocerebrosidase is shaking up the synucleinopathies. *Brain* (2014). doi:10.1093/brain/awu002
4. Orr-Urtreger, A. *et al.* Multicenter Analysis of Glucocerebrosidase Mutations in Parkinson's Disease. *N. Engl. J. Med.* **361**, 1651–1661 (2009).
5. Neumann, J. *et al.* Glucocerebrosidase mutations in clinical and pathologically proven Parkinson's disease. *Brain* (2009). doi:10.1093/brain/awp044
6. Gegg, M. E. *et al.* Glucocerebrosidase deficiency in substantia nigra of parkinson disease brains. *Ann. Neurol.* (2012). doi:10.1002/ana.23614
7. Parnetti, L. *et al.* Cerebrospinal fluid β-glucocerebrosidase activity is reduced in parkinson's disease patients. *Mov. Disord.* **32**, 1423–1431 (2017).
8. Atashrazm, F. *et al.* Reduced glucocerebrosidase activity in monocytes from patients with Parkinson's disease. *Sci. Reports 2018 81* **8**, 1–12 (2018).
9. Alcalay, R. N. *et al.* SMPD1 mutations, activity, and α-synuclein accumulation in Parkinson's disease. *Mov. Disord.* (2019). doi:10.1002/mds.27642
10. Gan-Or, Z. *et al.* The p.L302P mutation in the lysosomal enzyme gene SMPD1 is a risk factor for Parkinson disease. *Neurology* **80**, 1606–1610 (2013).
11. Foo, J. N. *et al.* Rare lysosomal enzyme gene SMPD1 variant (p.R591C) associates with Parkinson's disease. *Neurobiol. Aging* **34**, 2890.e13-2890.e15 (2013).
12. Mao, C. yuan *et al.* SMPD1 variants in Chinese Han patients with sporadic Parkinson's disease. *Parkinsonism Relat. Disord.* **34**, 59–61 (2017).
13. Dagan, E. *et al.* The contribution of Niemann-Pick SMPD1 mutations to Parkinson disease in Ashkenazi Jews. *Park. Relat. Disord.* **21**, 1067–1071 (2015).
14. Usenko, T. S. *et al.* Impaired Sphingolipid Hydrolase Activities in Dementia with Lewy Bodies and Multiple System Atrophy. *Mol. Neurobiol.* **59**, 2277–2287 (2022).
15. Flinn, L. J. *et al.* TigarB causes mitochondrial dysfunction and neuronal loss in PINK1 deficiency. *Ann. Neurol.* **74**, 837–847 (2013).

16. Larbalestier, H. *et al.* GCH1 Deficiency Activates Brain Innate Immune Response and Impairs Tyrosine Hydroxylase Homeostasis. *J. Neurosci.* **42**, 702–716 (2022).
17. Flinn, L. J. *et al.* TigarB causes mitochondrial dysfunction and neuronal loss in PINK1 deficiency. *Ann. Neurol.* **74**, 837–847 (2013).
18. Keatinge, M. *et al.* Glucocerebrosidase 1 deficient Danio rerio mirror key pathological aspects of human Gaucher disease and provide evidence of early microglial activation preceding alpha-synuclein-independent neuronal cell death. *Hum. Mol. Genet.* **24**, 6640–6666 (2015).
19. Keatinge, M. *et al.* Glucocerebrosidase 1 deficient Danio rerio mirror key pathological aspects of human Gaucher disease and provide evidence of early microglial activation preceding alpha-synuclein-independent neuronal cell death. *Hum. Mol. Genet.* **24**, 6640–6652 (2015).
20. Watson, L. *et al.* Ablation of the pro-inflammatory master regulator miR-155 does not mitigate neuroinflammation or neurodegeneration in a vertebrate model of Gaucher's disease. *Neurobiol. Dis.* (2019). doi:10.1016/j.nbd.2019.04.008
21. Keatinge, M. *et al.* CRISPR gRNA phenotypic screening in zebrafish reveals pro-regenerative genes in spinal cord injury. *PLOS Genet.* **17**, e1009515 (2021).
22. Hruscha, A. *et al.* Efficient CRISPR/Cas9 genome editing with low off-target effects in zebrafish. *Development* **140**, 4982–4987 (2013).
23. Wilkinson, R. N., Elworthy, S., Ingham, P. W. & van Eeden, F. J. M. A method for high-throughput PCR-based genotyping of larval zebrafish tail biopsies. *Biotechniques* (2013). doi:10.2144/000114116
24. Patro, R., Duggal, G., Love, M. I., Irizarry, R. A. & Kingsford, C. Salmon provides fast and bias-aware quantification of transcript expression. *Nat. Methods* (2017). doi:10.1038/nmeth.4197
25. Soneson, C., Love, M. I. & Robinson, M. D. Differential analyses for RNA-seq: Transcript-level estimates improve gene-level inferences [version 2; referees: 2 approved]. *F1000Research* (2016). doi:10.12688/F1000RESEARCH.7563.2
26. Love, M. I., Huber, W. & Anders, S. Moderated estimation of fold change and dispersion for RNA-seq data with DESeq2. *Genome Biol.* (2014). doi:10.1186/s13059-014-0550-8
27. Yu, G., Wang, L. G., Han, Y. & He, Q. Y. ClusterProfiler: An R package for comparing biological themes among gene clusters. *Omi. A J. Integr. Biol.* (2012). doi:10.1089/omi.2011.0118

28. Grabowski, G. A. Gaucher disease and other storage disorders. *Hematology / the Education Program of the American Society of Hematology. American Society of Hematology. Education Program* (2012). doi:10.1182/asheducation.v2012.1.13.3797921
29. Hannun, Y. A. & Obeid, L. M. Principles of bioactive lipid signalling: Lessons from sphingolipids. *Nat. Rev. Mol. Cell Biol.* **9**, 139–150 (2008).
30. Quinville, B. M., Deschenes, N. M., Ryckman, A. E. & Walia, J. S. A Comprehensive Review: Sphingolipid Metabolism and Implications of Disruption in Sphingolipid Homeostasis. *Int. J. Mol. Sci. 2021, Vol. 22, Page 5793* **22**, 5793 (2021).
31. Kim, S., Wong, Y. C., Gao, F. & Krainc, D. Dysregulation of mitochondria-lysosome contacts by GBA1 dysfunction in dopaminergic neuronal models of Parkinson's disease. *Nat. Commun. 2021 121* **12**, 1–14 (2021).
32. Magalhaes, J., Gegg, M. E., Migdalska-Richards, A. & Schapira, A. H. Effects of ambroxol on the autophagy-lysosome pathway and mitochondria in primary cortical neurons. *Sci. Reports 2018 81* **8**, 1–12 (2018).
33. Plotegher, N. *et al.* Impaired cellular bioenergetics caused by GBA1 depletion sensitizes neurons to calcium overload. *Cell Death Differ. 2019 275* **27**, 1588–1603 (2019).
34. Plotegher, N. & Duchen, M. R. Mitochondrial dysfunction and neurodegeneration in lysosomal storage disorders. *Trends Mol Med* **23**, 116–34 (2017).
35. Plotegher, N. & Duchen, M. R. Crosstalk between lysosomes and mitochondria in Parkinson's disease. *Front Cell Dev Biol* **5**, 2011–8 (2017).
36. Raimundo, N., Fernández-Mosquera, L., Yambire, K. F. & Diogo, C. V. Mechanisms of communication between mitochondria and lysosomes. *Int J Biochem Cell Biol* **79**, 345–9 (2016).
37. Niu, B. *et al.* Protecting mitochondria via inhibiting VDAC1 oligomerization alleviates ferroptosis in acetaminophen-induced acute liver injury. *Cell Biol. Toxicol.* **38**, 505–530 (2022).
38. Gillmore, T. *et al.* Dichotomy in hypoxia-induced mitochondrial fission in placental mesenchymal cells during development and preeclampsia: consequences for trophoblast mitochondrial homeostasis. *Cell Death Dis. 2022 132* **13**, 1–14 (2022).
39. Novgorodov, S. A. *et al.* Acid sphingomyelinase deficiency protects mitochondria and improves function recovery after brain injury. *J. Lipid Res.* **60**, 609–623 (2019).

40. Lee, J. K. *et al.* Acid sphingomyelinase modulates the autophagic process by controlling lysosomal biogenesis in Alzheimer's disease. *J. Exp. Med.* (2014). doi:10.1084/jem.20132451
41. Hagemann, N. *et al.* Homozygous Smpd1 deficiency aggravates brain ischemia/ reperfusion injury by mechanisms involving polymorphonuclear neutrophils, whereas heterozygous Smpd1 deficiency protects against mild focal cerebral ischemia. *Basic Res. Cardiol.* **115**, (2020).
42. Yu, Z. F. *et al.* Pivotal role for acidic sphingomyelinase in cerebral ischemia-induced ceramide and cytokine production, and neuronal apoptosis. *J. Mol. Neurosci. 2001 152* **15**, 85–97 (2000).
43. Canals, D. & Clarke, C. J. Compartmentalization of Sphingolipid metabolism: Implications for signaling and therapy. *Pharmacol. Ther.* **232**, (2022).
44. Ivanova, M. Clinical Medicine Altered Sphingolipids Metabolism Damaged Mitochondrial Functions: Lessons Learned from Gaucher and Fabry Diseases. *J. Clin. Med* **2020**, (1116).
45. Piccinini, M. *et al.* Deregulated sphingolipid metabolism and membrane organization in neurodegenerative disorders. *Mol. Neurobiol.* **41**, 314–340 (2010).
46. Katzy, R. E., Ferraz, M. J., Hazeu, M., Overkleeft, H. S. & Aerts, J. M. F. G. In situ glucosylceramide synthesis and its pharmacological inhibition analysed in cells by 13C5-sphingosine precursor feeding and mass spectrometry. *FEBS Lett.* **596**, 2400–2408 (2022).
47. Lelieveld, L. T. *et al.* Consequences of excessive glucosylsphingosine in glucocerebrosidase-deficient zebrafish. *J. Lipid Res.* 100199 (2022). doi:10.1016/J.JLR.2022.100199
48. Kim, M. J., Jeon, S., Burbulla, L. F. & Krainc, D. Acid ceramidase inhibition ameliorates α-synuclein accumulation upon loss of GBA1 function. *Hum. Mol. Genet.* (2018). doi:10.1093/hmg/ddy105

Figures

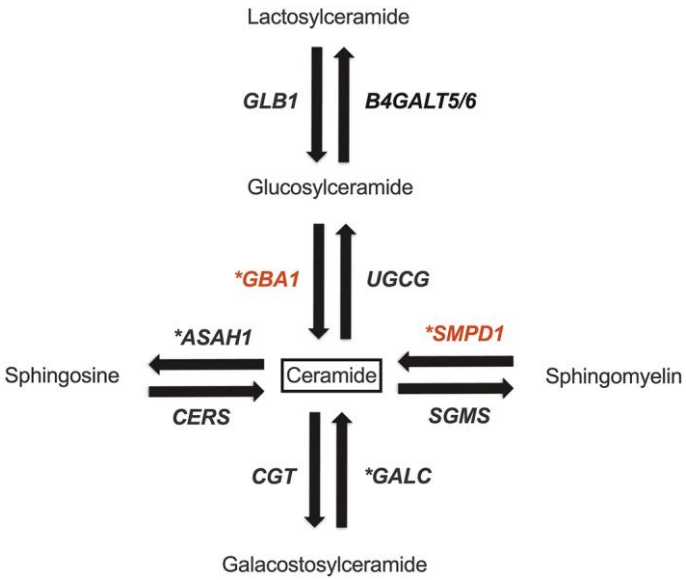

Fig. 1. A representative image of the ceramide pathway. Enzymes of the Ceramide pathway under study (*GBA1* and *SMPD1*) are highlighted in red, whilst *enzymes are linked to PD.

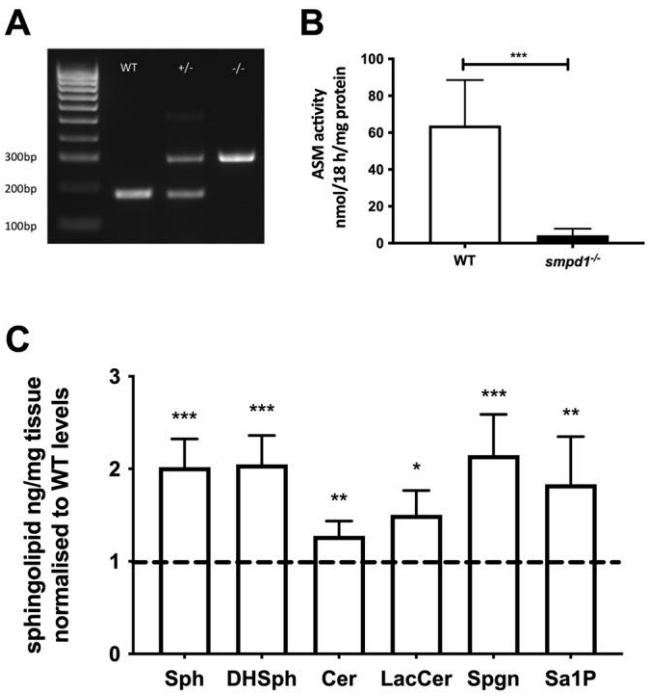

Fig. 2. Genetic and biochemical characterisation of the *smpd1*$^{-/-}$ mutant zebrafish line.

(A) Representative genotyping gel of the *smpd1*$^{-/-}$ alleles (5bp del and 136bp insertion) demonstrating WT, *smpd1*$^{+/-}$ and *smpd1*$^{-/-}$. (B) Acid sphingomyelinase (ASM) enzymatic activity compared to WT controls, n=6 larvae at 5 dpf per genotype, p=0.006 by Welch's t-test. (C) Quantification of sphingolipid metabolites, namely Sphingomyelin (Sph), dihydro-sphingomyelin (DHSph), ceramide (Cer), lactosylceramide (LacCer), Sphinganine (Spgn) and Sphinganine 1 phosphate (Sa1P). All metabolites shown are the C18 neuronal species. Data represented are the mean ±SD. ***p<0.001, **p<0.01 and *p<0.05 by two-tailed t-test.

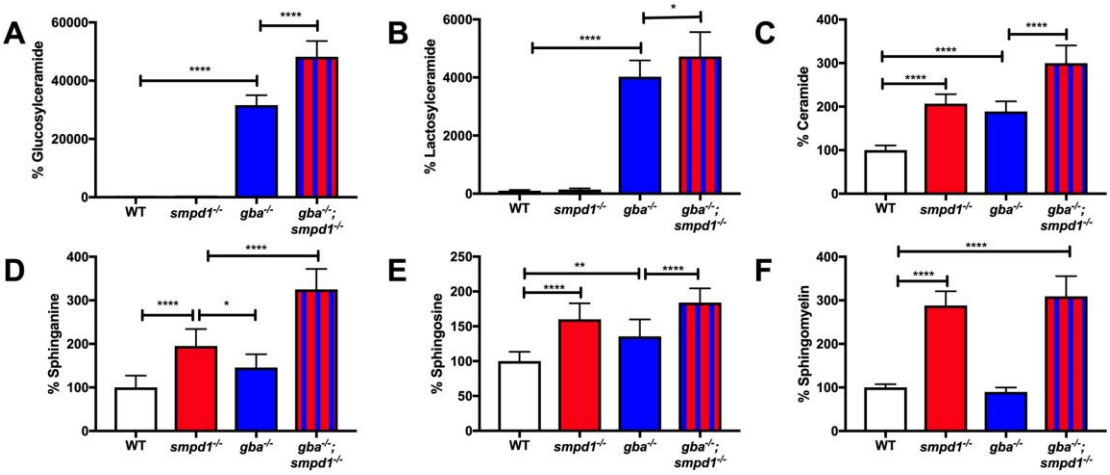

Fig. 3. Accumulation of key glycolipids across *gba1*$^{-/-}$ and *smpd1*$^{-/-}$ single mutant and *gba1*$^{-/-}$*; smpd1*$^{-/-}$ double mutant genotypes

(A) Glucosylceramide, (B) Lactosylceramide, (C) Ceramide (D), Sphinganine, (E) Sphingosine and (F) Sphingomyelin levels in WT, single mutant *gba1*$^{-/-}$ vs *smpd1*$^{-/-}$ zebrafish and *gba1*$^{-/-}$*; smpd1*$^{-/-}$ double mutant zebrafish. n=10 of 12 week old zebrafish brains used per group. Data represented are the mean ±SD. ****p<0.0001, ***p<0.001, **p<0.01 and *p<0.05 by 2 way Anova test with Tukey's multiple comparison.

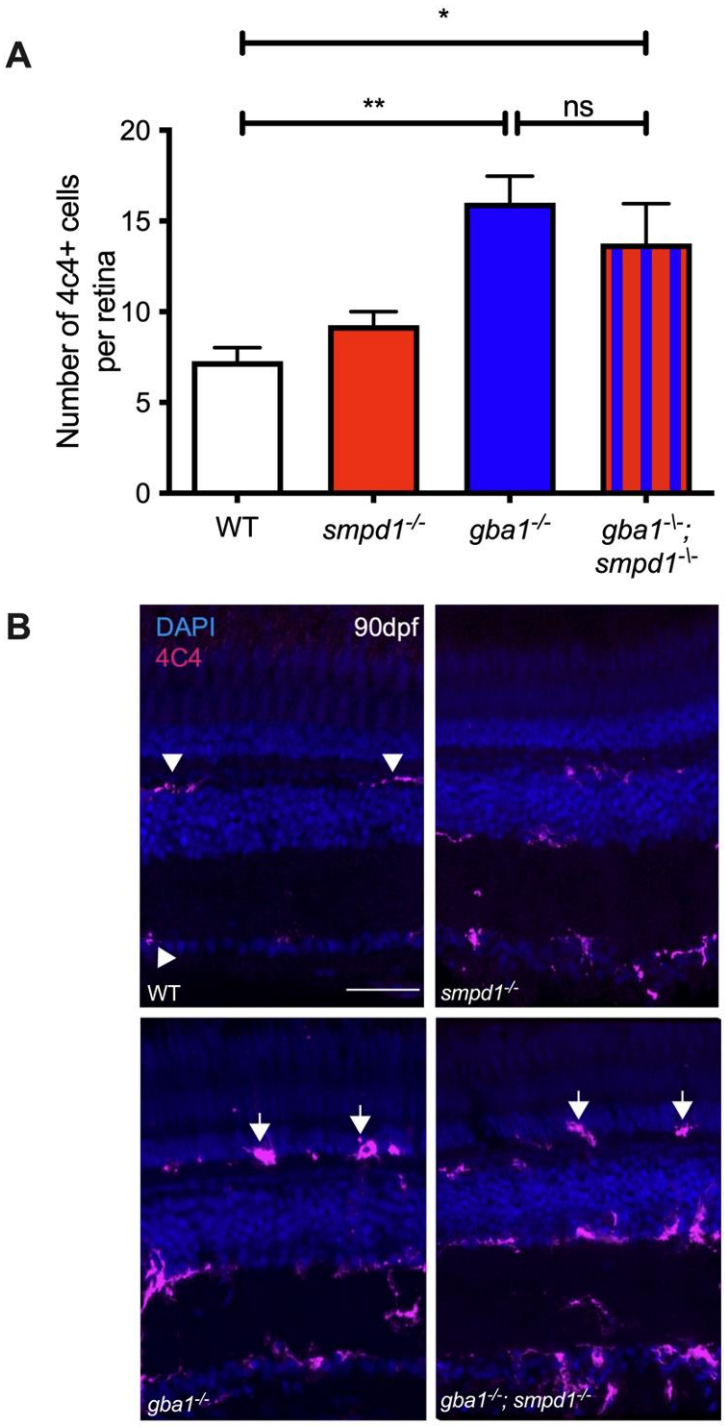

Fig. 4. Gaucher cell accumulation is present in the retina of *gba1*$^{-/-}$; *smpd1*$^{-/-}$ double mutants.

(A) Analysis of 4C4 positive cells within the retina reveals comparatively significant increases of ~50% in both *gba1*$^{-/-}$ (p=0.0026) and *gba1*$^{-/-}$; *smpd1*$^{-/-}$ double mutants (p=0.0193) compared to WT, despite enhancement of key glycolipids in the double mutants. 4C4 counts in the *smpd1*$^{-/-}$ were not statistically different to WT. Data represented are the mean ±SD. **p<0.01 and *p<0.05 by 2-way Anova test, n= 4 for

all groups. (B) 4C4 cells in the retina of the *gba1*$^{-/-}$ and *gba1*$^{-/-}$*; smpd1*$^{-/-}$ double mutants were localised throughout the retina and appeared larger and rounder (arrows), when compared to ramified WT 4C4 cells (arrowheads).

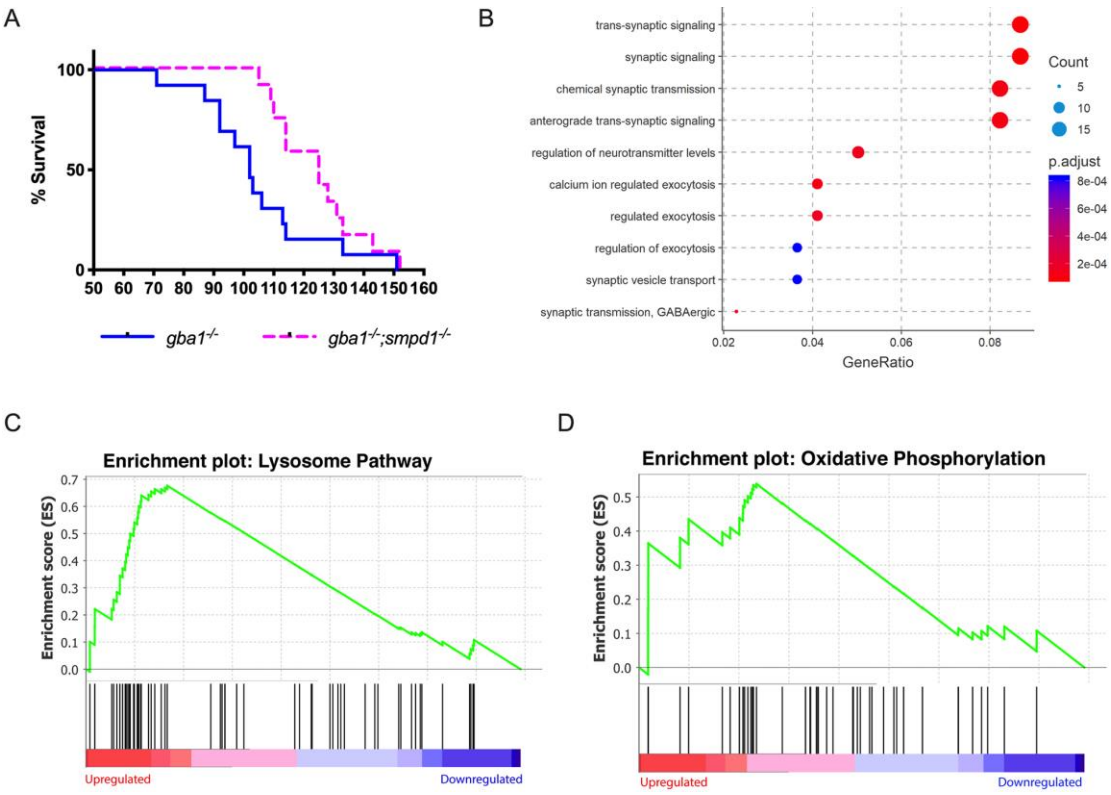

Fig. 5. Acid sphingomyelinase deficiency improves survival and rescues neuronal dysfunction in *gba*$^{-/-}$ zebrafish.

(A) Disease free survival analysis of *gba1*$^{-/-}$;*smpd1*$^{-/-}$ double-mutant (n=13) compared to *gba1*$^{-/-}$ single mutant zebrafish (n=12). p= 0.0055 by Gehan-Breslow-Wilcoxon test. Animals were culled for human reasons when they could no longer consistently maintain buoyancy (B) The Comparative gene ontology analysis indicates marked global impairment of neuronal function in *gba1*$^{-/-}$ but restoration of neuronal health in *gba1*$^{-/-}$;*smpd1*$^{-/-}$ **.** A differential expression analysis was first used to identify genes with statistically significant difference between *gba1*$^{-/-}$ and *gba1*$^{-/-}$;*smpd1*$^{-/-}$. Genes with adjusted p-value < 0.05 and log2 fold-change > 1 or <-1 were used to identify enriched biological processes amongst genes over- and under-expressed in *gba1*$^{-/-}$. ClusterProfiler identified significant enriched GO (gene ontology) terms within the gene expression changes which were plotted by GeneRatio (ratio of the differentially expressed genes in one particular GO term to the total number of differentially expressed genes). The lists of over- and under-expressed genes were analysed separately. Shown are the ten GO terms with highest gene ratios amongst under-expressed genes; all relating to key aspects of normal neuronal function and homeostasis. These pathways downregulated in *gba1*$^{-/-}$ compared to WT, were normalised in the double mutants. Each GO term is coloured according to the adjusted p-value and ranked according to gene ratio. The size of the point is then

scaled according to the number of differentially-expressed genes in the GO term. (C+D) Lysosomal pathway genes and oxidative phosphorylation pathway genes are upregulated in *gba*$^{-/-}$ but normalised in *gba1*$^{-/-}$*;smpd1*$^{-/-}$. The comparison of RNAseq-based transcription levels in the respective pathways between *gba*$^{-/-}$ and *gba1*$^{-/-}$*;smpd1*$^{-/-}$ revealed that both (C) lysosomal pathway genes and (D) oxidative phosphorylation pathway genes were enriched with marked upregulation of both pathways in *gba1*$^{-/-}$ compared to wild-type and *gba1*$^{-/-}$*;smpd1*$^{-/-}$. The x-axis ranks all differentially expressed genes based on the rank metric score from the most upregulated (left) to the most downregulated (right) for either pathway. The vertical black lines show the location of pathway genes in the entire ranked list from the *gba1*$^{-/-}$ expression changes, compared to WT and double mutants. The y-axis is the degree to which a set of pathway genes is overrepresented at the extremes (up or down-regulated) of the entire ranked list of all differentially expressed genes within the genome. A peak in enrichment score (green line) demonstrates an enrichment of pathway genes amongst all over- or under-represented genes. A sharp peak, demonstrates how highly upregulated each pathway is within the *gba1*$^{-/-}$ group compared to WT and double mutants.

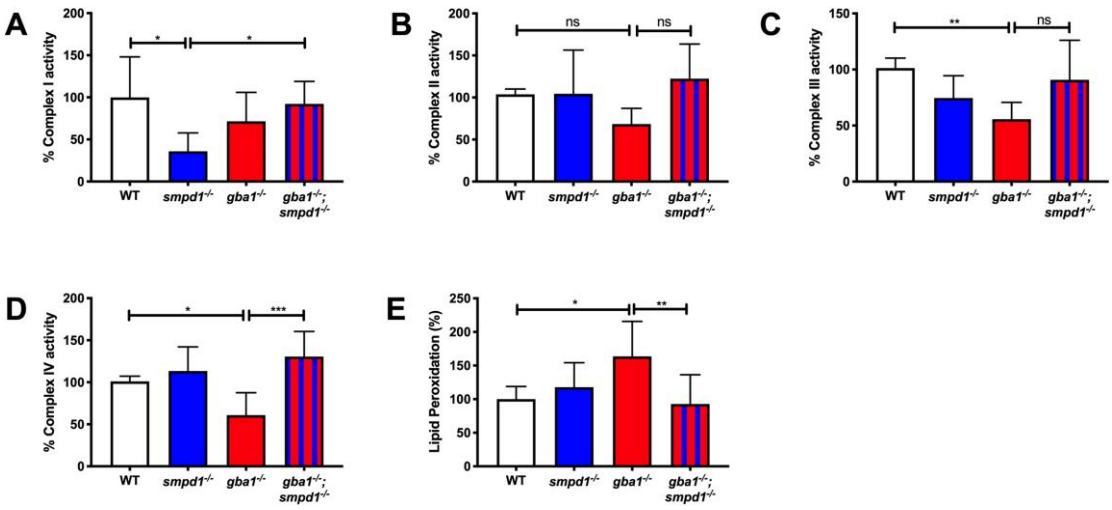

Fig. 6. Mitochondrial respiratory chain function and lipid peroxidation.

(A) Complex I activity was reduced in *smpd1*$^{-/-}$ by 64±34.77% compared to WT (p=0.0198). Complex I activity was normalised in *gba1*$^{-/-}$*;smpd1*$^{-/-}$ with an increase by 56±21.9% compared to *smpd1*$^{-/-}$ (p=0.0445). (B) Complex II activity was similar across the different genotypes (p>0.05). (C) Complex III activity was reduced in *gba1*$^{-/-}$ compared to WT by 45%±14.99 (p=0.0091) and increased by 35±35.2% in *gba1*$^{-/-}$*;smpd1*$^{-/-}$ compared to *gba1*$^{-/-}$ but this did not reach significance (p>0.05). (D) Complex IV activity was reduced in *gba1*$^{-/-}$ by 40%±26.79 compared to WT (p=0.0491), but completely rescued in *gba1*$^{-/-}$*;smpd1*$^{-/-}$ double mutants with an increase by 69±26.79% compared to *gba1*$^{-/-}$ (p=0.0005). For all mitochondrial complex activity measurements, 6 brains were used for each genotype. (E) Mitochondrial lipid peroxidation levels were increased 63±51% in *gba1*$^{-/-}$ compared to WT (p=0.0214), but reduced by 71±43.48% compared to *gba1*$^{-/-}$ and thus effectively normalised to WT levels in *gba1*$^{-/-}$*;smpd1*$^{-/-}$ double mutants (p=0.0094). For lipid peroxidation experiments, n= 6-8 zebrafish bodies were used for each genotype. Significance in both mitochondrial respiratory chain assays and lipid peroxidation levels was determined by two way ANOVA with Tukey's multiple comparison test using 12 week brain material. Data represented are the mean ±SD. ***p<0.001, **p<0.01 and *p<0.05.

smpd1 exon 3

CCGTGGTGGTTTCTACAGCGTGGAGGTTGAGCCTGGATTTGAAATAAAAAAATAATGCTAAAATTTAAATTTAAAT
AAAAATACAACATACAATACAAAATATATTTAAACCACAGAAAAACACTACAATTAAGCCACACATTAAACAAGTAA
AAACGCAGCNNTTTTTTTGTTTGAGGCTTGTGTCTCTGAACATGAACTTTTGCTCCAGAGAAAACTACTGGCTGA
TGGTGAACTCCACTGACCCAGCAGATCAGCTACAGTGGCTCATACAAATCCTGCAGGAGTCCGAGAACAAGGG
AGAGAAG

Fig. S1. CRISPR/Cas9 generated *smpd1* allele.

Using CRISPR/Cas9, we isolated a mutant allele in exon 3 containing a 5bp deletion (red script) with a 136bp insertion (blue script) leading to a frame shift and generation of a premature stop codon at codon 426 (full length WT smpd1: 676 amino acids).

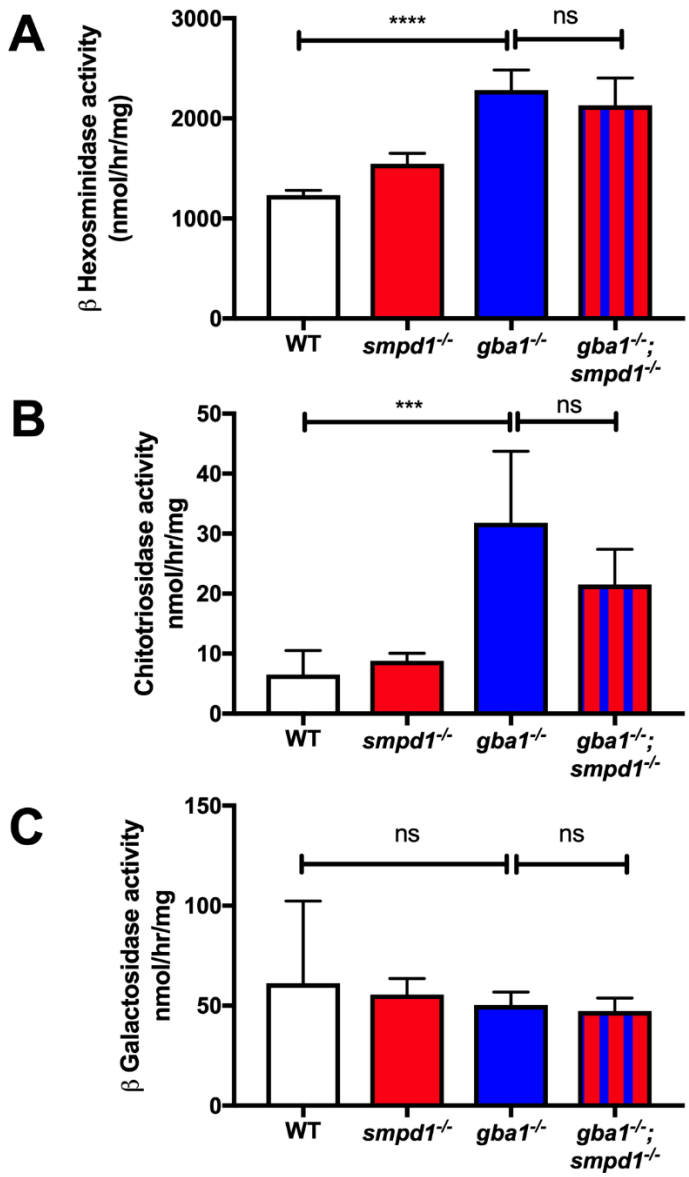

Fig. S2. GD biomarker activation is not substantially altered in *gba1*$^{-/-}$;*smpd1*$^{-/-}$.
(A) Hexosaminidase activity was not significantly changed between *smpd1*$^{-/-}$ and WT, but markedly elevated by 85% in *gba1*$^{-/-}$ (2284±200 nmol/hr/mg protein) compared to WT (1234±47.3nmol/hr/mg protein; p<0.0001). *gba1*$^{-/-}$;*smpd1*$^{-/-}$ displayed a similar increase in activity of 70% above WT levels (2131±272.2nmol/hr/mg protein, p<0.0001) compared to *gba1*$^{-/-}$. *(B)* Chitotriosidase activity was not significantly changed in *smpd1*$^{-/-}$ compared to WT, but increased in *gba1*$^{-/-}$ by 389% (31.8±11.95 nm/hr/mg protein, p=0.0002) compared to WT (6.5±4.0 nm/hr/mh protein) and by 230% in *gba1*$^{-/-}$;*smpd1*$^{-/-}$showed (21.5±5.1nm/hr/mg protein, p=0.0177) compared to WT. *(C)* Beta galactosidase activity in all genotypes showed comparable activities of approximately 50nm/hr/mg protein. Significance in all enzyme activities assays was determined by two way ANOVA with Tukey's multiple comparison test with an n of 5 per group using 12 week brain material. Data represented are the mean ±SD. ****p<0.0001, ***p<0.001, **p<0.01 and *p<0.05.

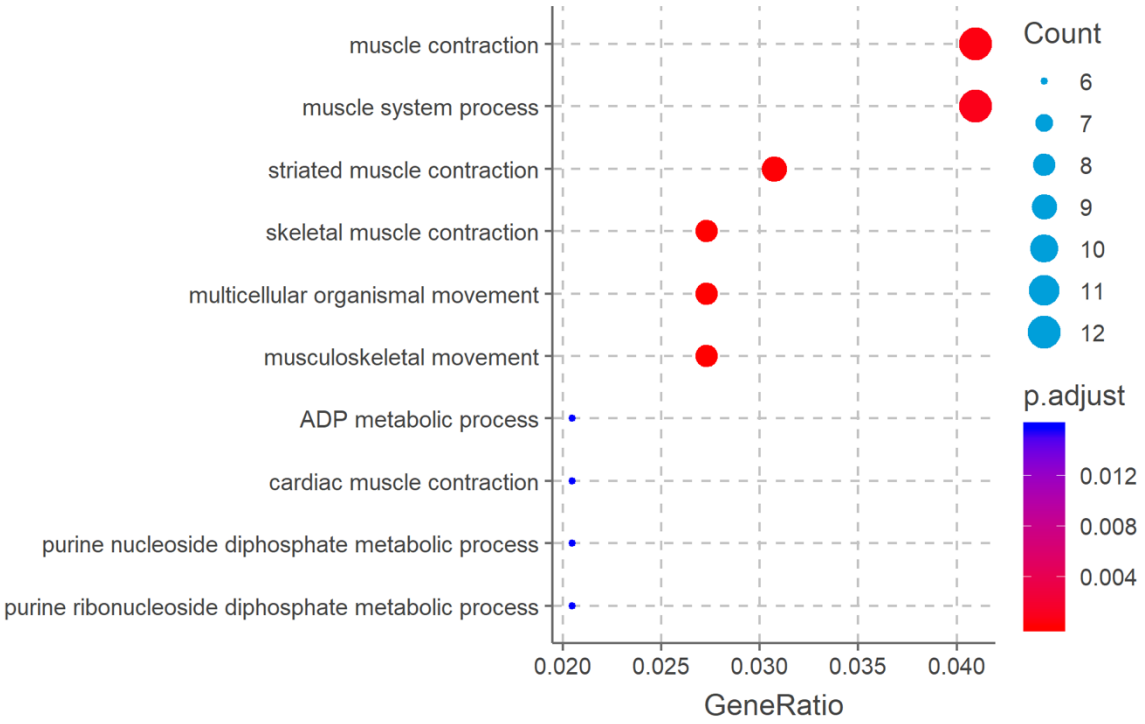

Fig. S3. Over-represented GO terms in the up-regulated genes. The top 10 GO terms as identified by ClusterProfiler from the list of statistically-significant genes (adjusted p-value < 0.05 and log2 fold-change > 1 or < -1 respectively. Each point is coloured according to the adjusted p-value for the GO term being over-represented, and the size of the point is scaled according to the number of differentially-expressed genes in the GO term. GO terms are ordered on the y-axis according to the size of the GO-term and adjusted p-value in the case of GO terms with the same number of genes.

Table S1. Observed and expected genotypes from *gba1*$^{+/-}$;*smpd1*$^{+/-}$ incrosses from 4 pooled clutches.

Genotype	*WT*	*gba1+/-; WT*	*gba1-/-; WT*	*WT; smpd1+/-*	*gba1+/-; smpd1+/-*	*gba1-/-; smpd1+/-*	*WT; smpd1-/-*	*gba1+/-; smpd1-/-*	*gba1-/-; smpd1-/-*	Total
n	14	48	15	26	48	27	23	35	15	251
Observed %	5.58%	19.12%	5.98%	10.36%	19.12%	10.76%	9.16%	13.94%	5.98%	100%
Expected %	6.25%	12.50%	6.25%	12.50%	25%	12.50%	6.25%	12.50%	6.25%	100%

Table S2. The leading-edge gene subset in lysosome pathway.

Symbol	Gene Name	Rank Metric Score
ctsl.1	cathepsin L.1	8.510105133
cd63	CD63 molecule	5.135530472
atp6ap1b	ATPase H+ transporting accessory protein 1b	5.114915371
lipf	lipase, gastric	3.06033802
fuca1.2	alpha-L-fucosidase 1, tandem duplicate 2	2.934919357
ctsba	cathepsin Ba	2.764246225
sftpbb	surfactant protein Bb	2.624561548
hexa	hexosaminidase A (alpha polypeptide)	2.622437954
zgc:110239	zgc:110239	2.503591537
acp5a	acid phosphatase 5a, tartrate resistant	2.363205671
gm2a	GM2 ganglioside activator	2.312668324
ctsa	cathepsin A	2.239866734
glb1	galactosidase, beta 1	2.198205709
dnase2b	deoxyribonuclease II beta	2.142905235
napsa	napsin A aspartic peptidase	1.98163259
atp6v0a1a	ATPase H+ transporting V0 subunit ca	1.948094964
ctsh	cathepsin H	1.844756842
manba	mannosidase, beta A, lysosoma	1.817932725
galns	galactosamine (N-acetyl)-6-sulfatase	1.797118545
dnase2	deoxyribonuclease II, lysosomal	1.73265183
npc1	Niemann-Pick disease, type C1	1.719917774
gnptg	N-acetylglucosamine-1-phosphate transferase subunit gamma	1.489329815
man2b1	mannosidase, alpha, class 2B, member 1	1.414416075
ap3b1a	adaptor related protein complex 3 subunit beta 1a	1.329013348
pla2g15	phospholipase A2, group XV	1.1423738
ppt1	palmitoyl-protein thioesterase 1 (ceroid-lipofuscinosis, neuronal 1, infantile)	1.051521778
atp6v0ca	ATPase H+ transporting V0 subunit ca	0.99467504

Table S3. The leading-edge gene subset in oxidative phosphorylation pathway.

Symbol	Gene Name	Rank Metric Score
atp6ap1b	ATPase H+ transporting accessory protein 1b	5.114915371
cox6a2	cytochrome c oxidase subunit 6A2	5.065165043
atp5pb	ATP synthase peripheral stalk-membrane	2.323343754
atp6v0a1a	ATPase H+ transporting V0 subunit a1a	1.948094964
atp6v0ca	ATPase H+ transporting V0 subunit ca	0.99467504
ndufb10	NADH:ubiquinone oxidoreductase subunit B10	0.839254677
ndufb6	NADH:ubiquinone oxidoreductase subunit B	0.643859327
ndufa11	NADH:ubiquinone oxidoreductase subunit A11	0.643721879
ndufv2	NADH:ubiquinone oxidoreductase subunit V2	0.574424922
cox4i1	cytochrome c oxidase subunit 4I1	0.573632479
sdhc	succinate dehydrogenase complex, subunit C, integral membrane protein	0.542427838
atp6v1g1	ATPase H+ transporting V1 subunit G1	0.497611314
cox4i2	cytochrome c oxidase subunit 4I2	0.428459734
cox5aa	cytochrome c oxidase subunit 5Aa	0.396667153
ndufa6	NADH:ubiquinone oxidoreductase subunit A6	0.356948555
ndufc2	NADH:ubiquinone oxidoreductase subunit C2	0.27688098

All videos were taken when the respective zebrafish were 12 weeks of age.

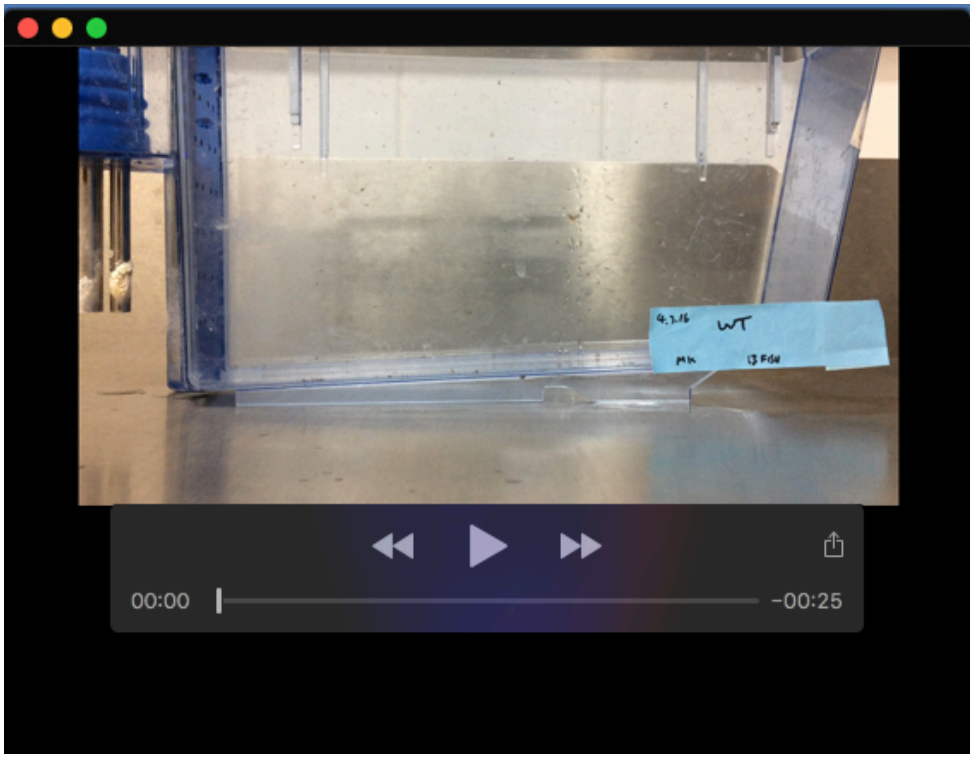

Movie 1. Swimming behaviour in WT. All adults placed into a novel tank swim to the bottom momentarily before resuming standard swimming, balance and buoyancy maintained.

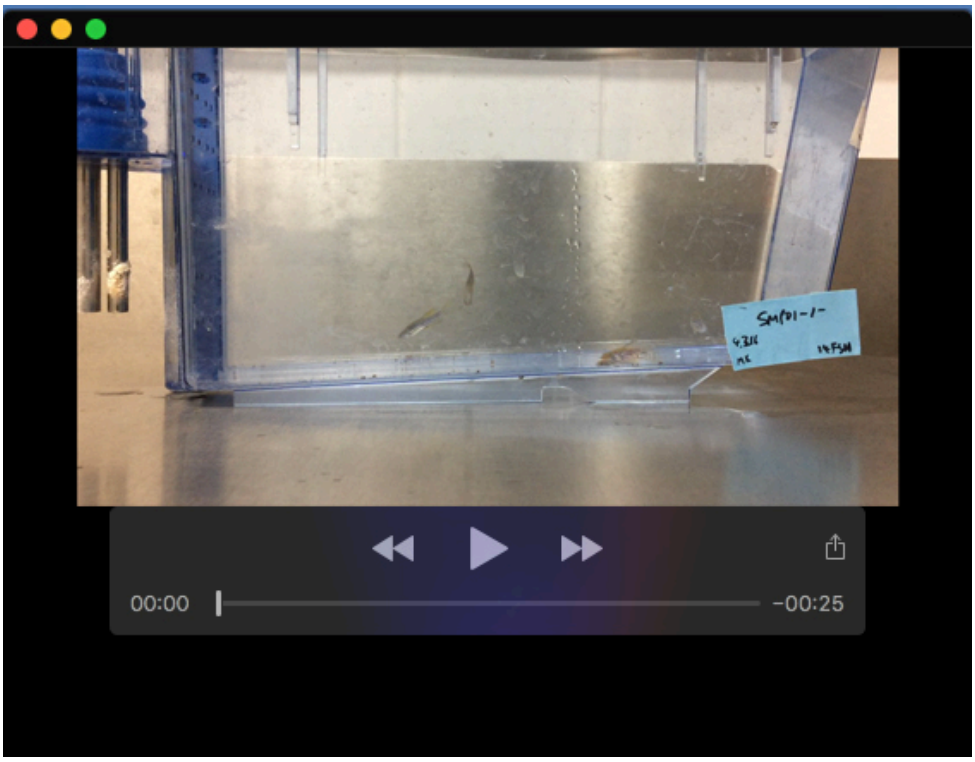

Movie 2. Swimming behaviour in *smpd*$^{-/-}$. All adults placed into a novel tank swim to the bottom momentarily before resuming standard swimming, balance and buoyancy maintained.

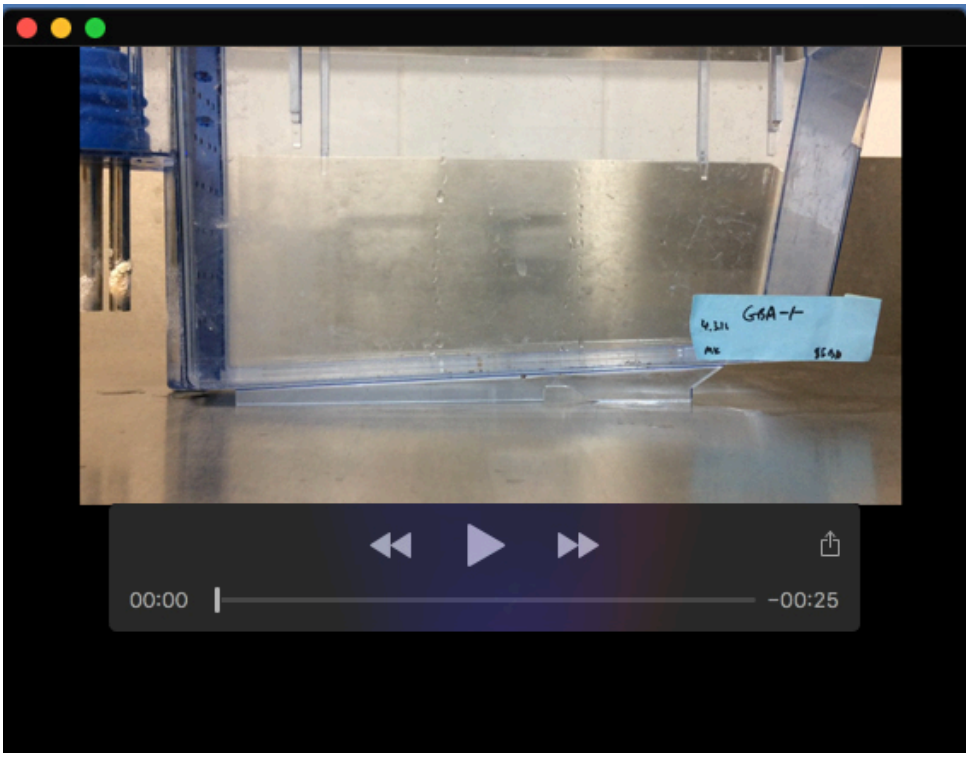

Movie 3. Markedly abnormal swimming behaviour in *gba*$^{-/-}$ with typical "corkscrew" swimming pattern. All adults placed into a novel tank swim in circular motions with balance and buoyancy defects. These increase with frequency and duration at end stage until they need to be culled for humane reasons.

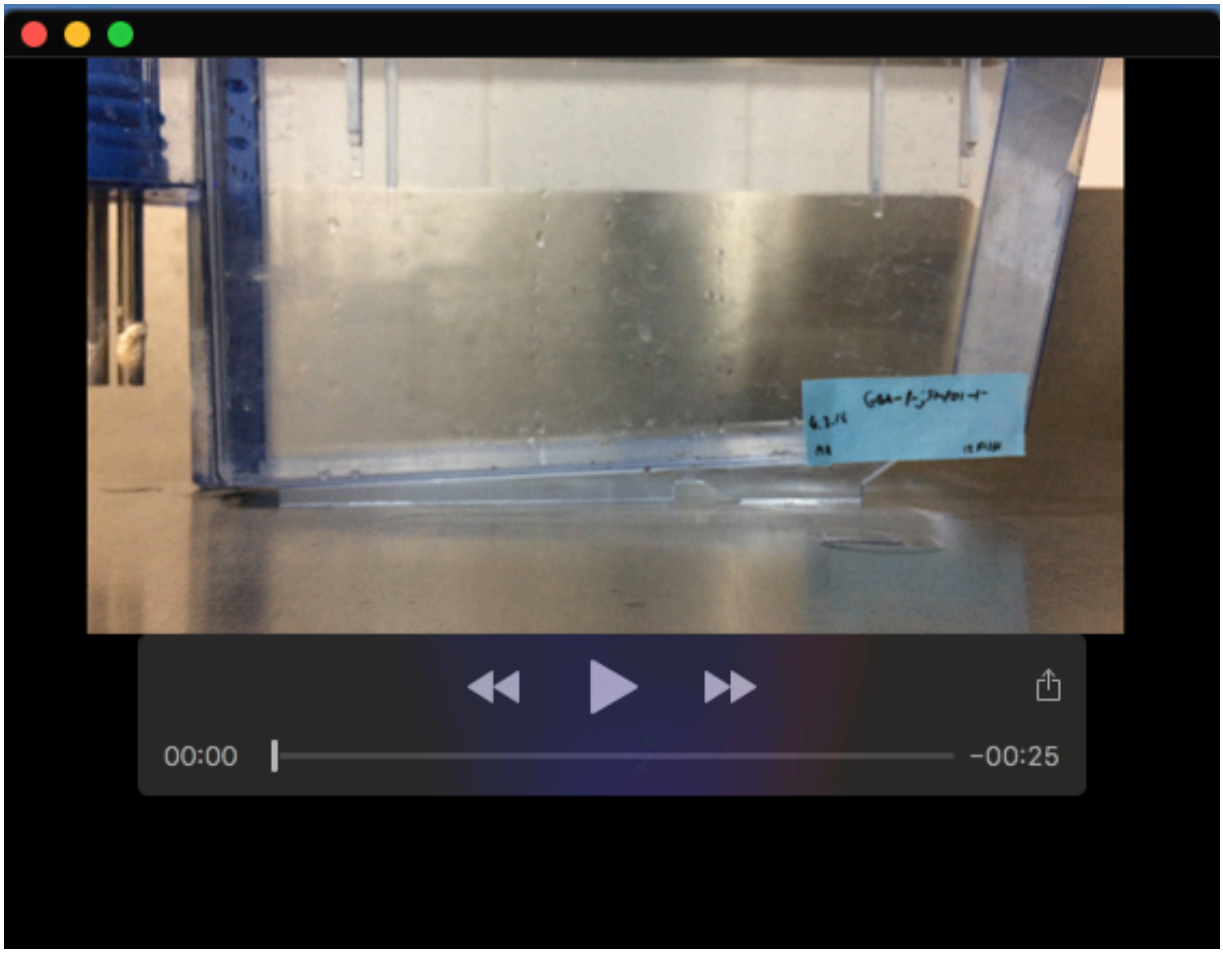

Movie 4. Swimming behaviour in *gba*$^{-/-}$;*smpd*$^{-/-}$. All adults placed into a novel tank swim to the bottom momentarily before resuming standard swimming, balance and buoyancy maintained.